Appl. Phys. B (2015) 119:165–175
DOI 10.1007/s00340-015-6013-4

Applied Physics B
Lasers and Optics

Monitoring CO_2 concentration and $\delta^{13}C$ in an underground cavity using a commercial isotope ratio infrared spectrometer

Sophie Guillon · Pierre Agrinier · Éric Pili

Received: 3 November 2014 / Accepted: 10 January 2015 / Published online: 3 February 2015

Abstract CO_2 stable carbon isotopes are very attractive in environmental research to investigate both natural and anthropogenic carbon sources. Laser-based isotope ratio infrared spectrometers (IRIS) allow in situ continuous monitoring of CO_2 isotopes, and therefore they have a potential for unprecedented understanding of carbon sources and dynamics with a high temporal resolution. Here we present the performance assessment of a commercial IRIS analyzer, including the measurement setup and the data processing scheme that we used. Even if the analyzer performs 1-Hz measurements, an integration time of the order of 1 h is commonly needed to obtain acceptable precision for $\delta^{13}C$. The main sources of uncertainty on $\delta^{13}C$ come from the concentration dependence and from the temporal instability of the analyzer. The method is applied to the in situ monitoring of the CO_2 carbon isotopes in an underground cavity (Roselend Natural Laboratory, France) during several months. On a weekly timescale, the temporal variability of CO_2 is dominated by transient contamination by human breath. Discarding these anthropogenic contaminations, CO_2 and $\delta^{13}C$ backgrounds do not show diurnal or seasonal fluctuations. A CO_2 flux released into the tunnel by the surrounding rocks is measured. The carbon isotope composition of this CO_2, identified with a Keeling plot, is consistent with a main production by microbial respiration and a minor production from weathering of carbonate minerals. The presented instrument and application study are relevant to cave monitoring, whether to understand CO_2 dynamics in visited and/or painted caves for preservation purposes or to understand paleoclimate recording in speleothems.

S. Guillon (✉) · É. Pili
CEA, DAM, DIF, 91297 Arpajon, France
e-mail: sguillon@ipgp.fr

S. Guillon · P. Agrinier
Institut de Physique du Globe de Paris, Sorbonne Paris Cité, Univ Paris Diderot, UMR 7154 CNRS, 75005 Paris, France

1 Introduction

CO_2 stable isotopes are widely used to study the sources and fates of carbon in the atmosphere, hydrosphere and geosphere, as well as the exchanges between these reservoirs.

For around 10 years, commercial analyzers have been available, based on isotope ratio infrared spectroscopy (IRIS). These analyzers have a high temporal resolution and low power consumption and allow long-term continuous in situ monitoring of carbon isotopes in the field, which was not possible with classical isotope ratio mass spectrometry (IRMS). Several IRIS analyzers now exist for measuring CO_2 carbon and oxygen isotopes that are based on different technologies [1–5]. However, studies using such commercial analyzers have revealed difficulties to obtain reliable and accurate data. They also emphasized the need for users to thoroughly assess the analyzers' performance in the field and to establish calibration strategies to correct raw data for the identified biases [3, 6]. Commercial IRIS instruments are often designed for atmospheric monitoring and present good accuracy at low and not strongly variable CO_2 concentration [3, 7, 8]. But there is also a need for carbon isotope monitoring at higher and more variable concentrations, in volcanic [2] or underground [9] environments, as well as for soil [10] and fermentation plants monitoring [11].

Here we focus on CO_2 carbon isotope monitoring in geological media, where the CO_2 concentration is large and is known to be variable [12, 13]. First, the performances of the commercial analyzer were determined in the laboratory in terms of precision, linearity and response time, allowing

to establish a data processing method. Then, we apply the method to the monitoring of CO_2 in the atmosphere of an underground cavity during several months. The carbon cycle is investigated at the Roselend Natural Laboratory (French Alps) using isotope ratios, in order to identify the carbon sources and fates, to quantify respective fluxes, to appreciate the dynamics of the carbon system and to explain it in terms of forcing factors. Crystalline rocks, present around the Roselend tunnel, have indeed been showed to be net sources of CO_2 to the atmosphere [14]. This article aims to show what can be done with supposedly easy-to-use commercial instruments and to emphasize the work that is required to obtain accurate and reliable data as well as the numerous caveats and the large uncertainties.

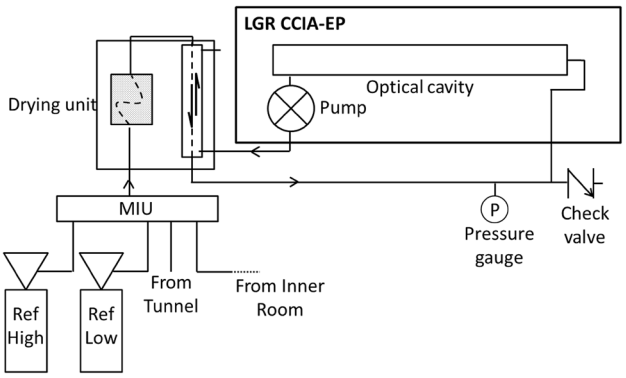

Fig. 1 Experimental setup used for in situ monitoring of CO_2 concentration and $\delta^{13}C$ in the Roselend Natural Laboratory. See text for details. In the drying unit, the *dashed lines* stand for Nafion® tubings, the *shaded zone* for Drierite®

2 Materials and methods

2.1 Commercial laser-based isotope analyzer

In this study, we used the Los Gatos Research CCIA-EP (CO_2 Carbon Isotope Analyzer-Enhanced Performance, purchased in mid-2011), a commercial IRIS analyzer based on off-axis integrated cavity output spectroscopy. The technique is described in detail in [15]. This is an enhanced performance version of the instrument presented in [6]. It is mainly characterized by a better thermal insulation, aimed at decreasing the observed large sensitivity to external temperature variations. CO_2 concentration, carbon and oxygen isotopes, as well as water content, are measured using absorption lines around 2.05 µm (D. Baer, pers. comm.). Pressure and temperature in the optical cavity are constant at 45.20 ± 0.05 °C and 39 torr, respectively. Air flow through the instrument is driven by its internal diaphragm pump and is around 0.5 L min^{-1}. Data acquisition is done at 1 Hz.

Here, we mainly focus on the CO_2 carbon isotope measurement because, from our point of view, oxygen isotope measurement with this instrument still requires improvement in precision and in the availability of calibration standards. CO_2 carbon isotope composition is reported as $\delta^{13}C$ versus VPDB standard (Vienna Pee Dee Belemnite), and reported in per mil (‰), where

$$\delta^{13}C(‰) = \left(\frac{R_{\text{sample}}}{R_{\text{VPDB}}} - 1\right) \times 1{,}000\,‰ \quad (1)$$

where $R = ([^{13}C]/[^{12}C])_{CO_2}$.

2.2 Reference gases

Reference gases (Air Products) were used for the performance assessment of the analyzer in the laboratory as well as for calibration during field monitoring. For the reference gases to be as close as possible to the measured gases, they consisted of CO_2 in a matrix with 78 % N_2, 21 % O_2 and 1 % Ar. Both these reference gases and the sample gases are passed through a drying unit, to keep moisture as constant and as low as possible in the analyzer. This drying unit (Fig. 1) consists in a 30-cm Nafion® tubing embedded in a desiccant (Drierite®) mounted in line with another Nafion® tubing embedded in a stainless tube, with a counterflow of dry air provided by the exhaust of the analyzer. This drying unit works as a true drying unit for the moist sample gases (with average moisture content of 12,000 ppm), whereas it actually acts as a humidifier for the dry reference gas streams. The average moisture content downstream this drying unit is of few thousands ppm. Reference gases A, F and G (Table 1) were used for the performance assessment in the laboratory. Reference gases B–E were used for calibration during field monitoring. CO_2 concentrations of these reference gases correspond to the minimum and maximum values of CO_2 concentration expected during monitoring, about 350–900 ppm. All CO_2 and H_2O concentrations are reported in parts per million per volume, noted ppm for the sake of brevity. CO_2 concentrations are known within 0.5 % from the certified values given by the manufacturer. The $\delta^{13}C$ values of these reference gases were measured by CF-IRMS (Gas Bench II and DeltaPlusXP, Thermo Finnigan) at the Institut de Physique du Globe de Paris. Precision on $\delta^{13}C$ values is better than 0.3 ‰.

2.3 Performance assessment in the laboratory

Three tests were conducted in the laboratory to assess the performance of the analyzer.

First, the Allan–Werle deviation is a widely accepted tool in the diode-laser spectroscopy community that quantifies the intrinsic precision of the analyzer and highlights its

Table 1 CO_2 concentration and carbon isotope composition $\delta^{13}C$ of the reference gases used in this study

	$[CO_2]$ (ppm)[a]	$\delta^{13}C$ (‰)[b]
A	300.5	-35.5 ± 0.2
B	392.0	-42.4 ± 0.4
C	399.2	-35.8 ± 0.8
D	500.6	-36.4 ± 0.3
E	898.5	-35.5 ± 0.1
F	2,002	-35.2 ± 0.4
G	17,800	-39.6 ± 0.2

[a] Determined gravimetrically by the manufacturer (Air Products), $1\sigma = 0.5$ %

[b] Determined by CF-IRMS at Institut de Physique du Globe de Paris

stability or drift, in order to determine data integration time and frequency of calibrations. It is defined as the deviation between adjacent data as a function of data averaging time [16, 17]:

$$\sigma^2_{\text{Allan}}(\tau) = \frac{1}{2}\left\langle \left(\underset{t_k+\tau}{\bar{\delta}} - \underset{t_k}{\bar{\delta}} \right)^2 \right\rangle, \quad \underset{t_k}{\bar{\delta}}(\tau) = \frac{1}{\tau}\int_{t_k}^{t_k+\tau} \delta(t)dt \quad (2)$$

where τ is averaging time, $\langle\rangle$ is the expectation value, and k and $k + \tau$ are adjacent averaged data. The Allan–Werle deviation was determined from 2-h-long continuous measurements of reference gases, for CO_2 concentration as well as for carbon and oxygen isotope compositions. This was done for three reference gases (A, F and G) with concentrations of 300, 2,002 and 17,800 ppm CO_2.

Second, the response time of the analyzer following a stepwise change of concentration and isotope composition of the inlet gas was determined by switching between two reference gases (A–F, A–G and F–G). The response time determines the high-frequency limit of the CO_2 dynamics that can be retrieved with this analyzer.

Third, the $\delta^{13}C$ dependence on CO_2 concentration is known to be one of the largest sources of uncertainty for IRIS analyzers [3, 7, 9, 18, 19] and needs to be carefully checked. Reference gases with 17,800 as well as 2,002 ppm CO_2 concentrations (F and G, Table 1) were stepwise diluted by CO_2-free synthetic air with 78 % N_2, 21 % O_2 (Air Products), using two mass flow controllers (SLA5850S, Brooks, range 1 L min^{-1}). We assume that the mass flow controllers induce no fractionation.

The enhanced version of the Los Gatos Research IRIS analyzer has an improved thermal insulation, and measurements were taken either in the laboratory where temperature is controlled (at ±0.3 °C) or in an underground tunnel where the temperature is naturally very stable at 7.2 ± 0.2 °C. We therefore did not have to investigate the effect of ambient temperature variations on the measurement, which has nonetheless been shown to be a large source of drift and error [6, 7].

2.4 Monitoring of CO_2 carbon dynamics in an underground cavity

The study site is the Roselend Natural Laboratory [20], located in the French Alps. This underground research laboratory mainly consists in a horizontal tunnel hosted in bare fractured crystalline rocks. The tunnel is 128-m long, with a 2.4-m diameter. It is naturally ventilated by ambient atmospheric air at its open end. All along the tunnel, water is dripping from rocks. At mid-length of the tunnel, a side excavation of approximately 9 m length and 3 m width, called Inner Room, was roughly isolated by a steel door and sealing foam.

An IRIS analyzer had already been used at this site to measure CO_2 carbon dynamics in a small borehole [6]. Here we present a long-term monitoring of CO_2 dynamics in the tunnel and in the Inner Room. The analyzer was installed in a portion of the tunnel where the water drip rate is very low, so that it did not require to be especially protected.

The experimental setup of the analyzer for in situ continuous monitoring is shown in Fig. 1. A multi-inlet unit with eight ports (MIU, Los Gatos Research) was used to automatically switch at selected time periods between the streamlines, one from the open tunnel, one from the isolated Inner Room and two from the non-diluted reference gases (B and E in 2013, C and D in 2014). The drying unit was installed between the MIU outlet and the analyzer inlet (Fig. 1). Air was drawn from the tunnel and from the reference gas cylinders through 6.4-mm external diameter PFA tubing. A similar, 8-m long tubing, passing through the rock above the Inner Room's door, was used to draw air from the Inner Room. This tubing was inserted 2 m inside the Inner Room. A pressure gauge and a 10-psi check valve (Swagelok®) were fixed at the inlet of the CCIA-EP, in order to prevent any overpressure that would damage the analyzer (Fig. 1).

During the monitoring period, from April to June 2013, and then from May to July 2014, the analyzer was measuring at 1-Hz rate the CO_2 concentration and $\delta^{13}C$ of air from the tunnel or from the Inner Room. The MIU automatically switched between the two sample streamlines every 2 h, while the high- and low-concentration reference gases were measured every 8 h during 5 min. The concentration dependence of the analyzer was checked manually every month, following the protocol presented above. This protocol has been defined according to the results of experiments about performance of the analyzer. No data were recorded during several periods due to various types of failures (laser drift, software error and power surge).

3 Results

3.1 Performance of the analyzer

The Allan–Werle deviations for $\delta^{13}C$ and $\delta^{18}O$ were calculated following Eq. (1) [16, 17] and are presented in Fig. 2. Precision, given by the Allan–Werle deviation, increases with averaging time due to white noise averaging and also increases when CO_2 concentration increases (Fig. 2). At CO_2 concentration higher than 2,000 ppm, the optimum precision ($\sigma = 0.05$ ‰) for $\delta^{13}C$ is reached for an averaging time of 200 s; while at 300 ppm, the optimum precision ($\sigma = 0.08$ ‰) is only reached after 900 s. For longer averaging time, precision gets worse due to long-term drift. A good precision ($\sigma = 0.02$ %) on CO_2 concentration is obtained at 60 s averaging time. The precision on $\delta^{18}O$ measurement (Fig. 2b) is one order of magnitude worse than of $\delta^{13}C$ (Fig. 2a). An averaging time of 20 min is thus required to obtain a precision of $\sigma = 0.4$ ‰ for $\delta^{18}O$.

As several combinations of reference gases were used to determine the response time of the analyzer, data were first normalized to the difference in concentration or isotope composition between the two measured gases. How fast the analyzer reaches a new steady state after a stepwise change in inlet composition is quantified using the 5–95 % response time [21], i.e., the time needed for the measurement to go from 5 to 95 % of the difference between the initial and final values. After a change in the sample gas concentrations and delta values at the inlet of the multi-inlet unit, the analyzer response remains stable and equal to the initial values for some time, while the inlet gas has already been changed. This delay is interpreted to be due to piston-like propagation of air through the tubing between the multi-inlet switching valve and the inlet of the optical cavity in the analyzer. The average delay that was obtained for this propagation is 20.3 ± 1.7 s and does not depend on the difference in concentration or isotope composition. Then, a classical exponential increase or decrease response was observed, with a 5–95 % response time on average of 30 s for CO_2 concentration and 60–100 s for isotope composition values. This response time suggests the existence of dead volumes in the instrument that take some time to be purged. Response time cannot be reduced with the commercial analyzer used in this study, because cell pressure and flow rate cannot be changed.

Stepwise dilution with zero air was performed and repeated at various time intervals, for the two reference gases having 2,002 and 17,800 ppm CO_2 concentrations (F, G, Table 1). Results for $\delta^{13}C$ are presented in Fig. 3. The dependence of $\delta^{13}C$ on the CO_2 concentration can be up to 19 ‰ in the concentration range 300–17,800 ppm, and 6 ‰ in the more limited concentration range 300–1,000 ppm. At high CO_2 concentrations, typically higher than 5,000 ppm, the dependence law is linear (Fig. 3a), with quite a good

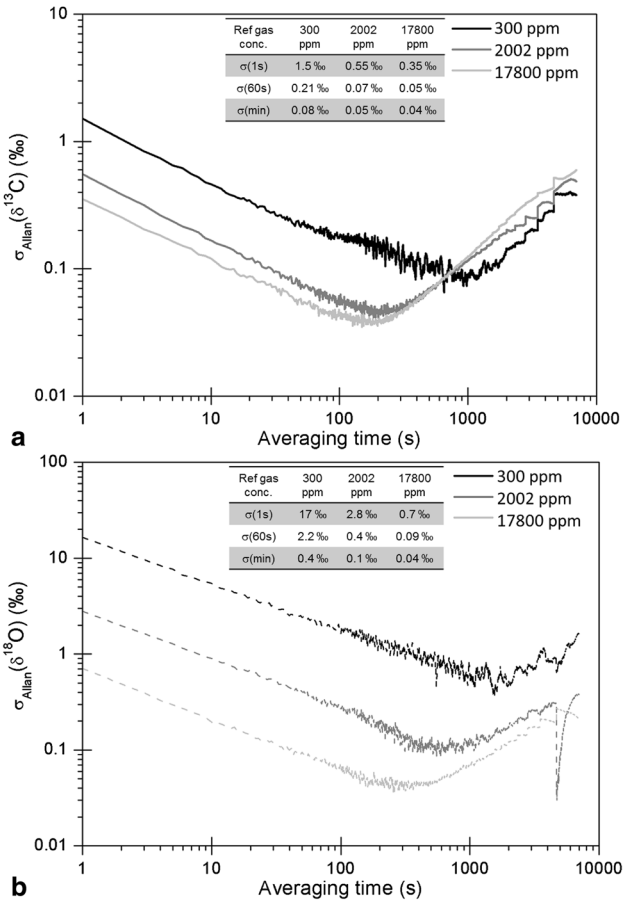

Fig. 2 Allan plots for **a** $\delta^{13}C$ and **b** $\delta^{18}O$ of CO_2 from three reference gases. Allan–Werle deviations were computed following [17], for reference gases with concentrations of 300 ppm (*black*), 2,002 ppm (*dark gray*) and 17,800 ppm (*light gray*). Precision (σ) for 1 s and 60 s averaging times, as well as best precision (σ_{min}), are summarized in tables

reproducibility of the slope (0.0013 ± 0.0002 ‰ ppm^{-1}). At low CO_2 concentration, the situation is more complex. The dependence law appears to be stable at the hourly timescale (data not shown). At the daily timescale, a strong variability is observed (Fig. 3b). However, the dependence law keeps the same shape, being randomly shifted (up to 5 ‰ in 24 h). This leads to propose a simple way to handle this correction while using the analyzer unattended: the shift and global shape of the law are evaluated every few hours by automatically running at least two reference gases, while the more detailed shape of the dependence law must be checked every month by manually running a stepwise dilution of a reference gas.

3.2 Calibration and data processing

For each data set acquired in the field, temperature in the optical cavity was monitored. It was stable within

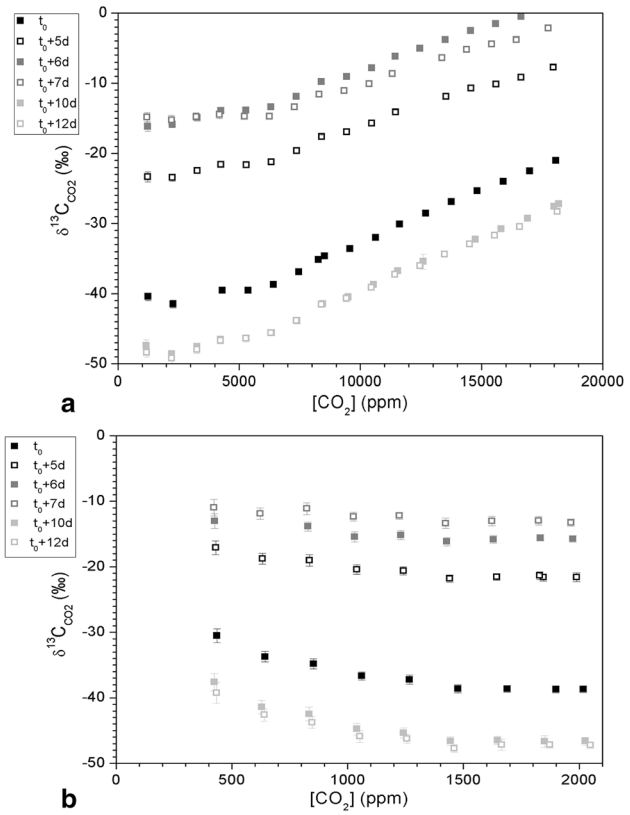

Fig. 3 Concentration dependence of $\delta^{13}C$ measurement. **a** up to 17,800 ppm CO_2; **b** in the range 400–2,000 ppm CO_2. $\delta^{13}C$ is reported as raw values. Stepwise dilutions of reference gases G (**a**) and F (**b**) with CO_2-free air were repeated several times

±0.05 °C; therefore, no temperature correction was applied. While water concentration measured in the tunnel without using the drying unit was around 12,000 ppm, the measured water concentration using the drying unit slowly increased from 1,000 to 5,000 ppm during the whole measurement period, indicating the decreasing efficiency of the drying unit as the Drierite got progressively saturated. Longer Nafion tubing and more Drierite may mitigate this problem. Humidity levels were on average 1,000 ppm higher in samples than in reference gases. These humidity values, reduced and similar in sample and reference gases, allow us to reduce uncertainty linked to measurement and calibration.

Based on the above performance and concentration dependence measured in the laboratory, as well as on methodologies proposed by others [3, 7], the following calibration method was used to process the raw data. Raw data files from the CCIA-EP analyzer were first handled with a program written in Fortran, in order to:

1. sort out the data for the two samples and the two reference gases that were measured,
2. remove 2 min of data after switching from one sample to another,
3. reduce the amount of data by averaging them on a 1-min basis.

Although the 1-min averaging of the raw data does not give the best precision, as shown by the Allan–Werle deviation, this averaging time was chosen in order to reduce the large amount of data acquired at 1 Hz, while keeping a good temporal resolution. The two measured reference gases are used for calibrating concentrations as well as $\delta^{13}C$ values, taking into account the dependence on concentration. From 300 s of measurement of the two reference gases conducted every 8 h, the first 100 s are removed, and CO_2 concentration and $\delta^{13}C$ values are averaged over the last 200 s. This leads to one average value of CO_2 concentration and $\delta^{13}C$ every 8 h, for each reference gas. A linear time interpolation is then used to reconstruct the time series of reference CO_2 concentration and $\delta^{13}C$ with a 1-min time step.

A linear calibration of the raw CO_2 concentration ($[CO_2]_{meas}$) is then applied:

$$[CO_2]_{corr} - [CO_2]_{meas} = q(t) \cdot [CO_2]_{meas} + r(t) \quad (3)$$

where $[CO_2]_{corr}$ is the corrected CO_2 concentration and $q(t)$ and $r(t)$ are the two calibration parameters, which vary with time. These parameters are determined at each time step (i.e., every minute in the presented case) from the interpolated CO_2 concentrations for the two reference gases. The corrections for the concentration dependence on $\delta^{13}C$ measurement, as well as calibration of $\delta^{13}C$ value against the international PDB scale, are then applied. As we have no physical model for the concentration dependence law, and based on the concentration dependence measurements (Fig. 3b), we chose a linear relation between the shift on $\delta^{13}C$ and the CO_2 concentration:

$$\left(\delta^{13}C\right)_{corr} - \left(\delta^{13}C\right)_{meas} = u(t) \cdot [CO_2]_{corr} + v(t) \quad (4)$$

where $(\delta^{13}C)_{meas}$ is the raw value of carbon isotope composition given by the analyzer, $(\delta^{13}C)_{corr}$ is the corrected value in the PDB scale, $[CO_2]_{corr}$ is the concentration after calibration using Eq. (3), and $u(t)$ and $v(t)$ are two calibration parameters which vary with time. These parameters are determined from the interpolated $\delta^{13}C$ values for the two reference gases. This relation is valid and can be applied only for CO_2 concentrations in the range 400–1,000 ppm, where the concentration dependence law was shown to be linear (Fig. 3b). Corrected CO_2 concentration and $\delta^{13}C$ data are finally averaged with a 1-h time step. This time step gives a good accuracy, with a temporal resolution that is high enough to investigate most dynamics. The calibration and averaging procedures were automated using a MATLAB program.

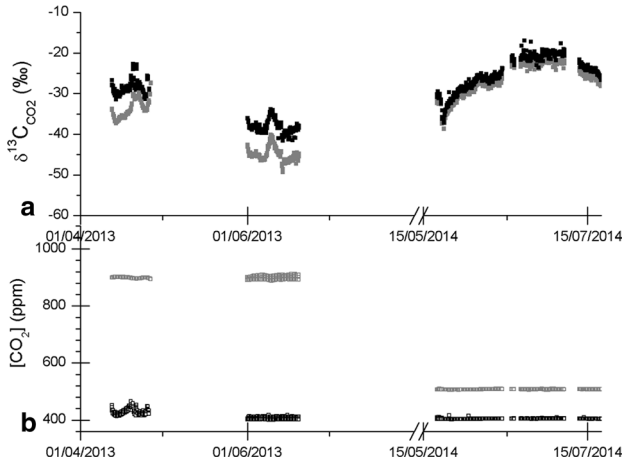

Fig. 4 Reference gases measurements of $\delta^{13}C$ (**a**) and CO_2 concentration (**b**) during a total of 3 months (April and June 2013, May to July 2014). The analyzer was set up in the tunnel. Two reference gases with high (*gray*, E in 2013, D in 2014) and low (*black*, B in 2013, C in 2014) CO_2 concentrations were measured and used for calibration. See Table 1 for their CO_2 concentration and $\delta^{13}C$ values. Reported data are 1-min averages

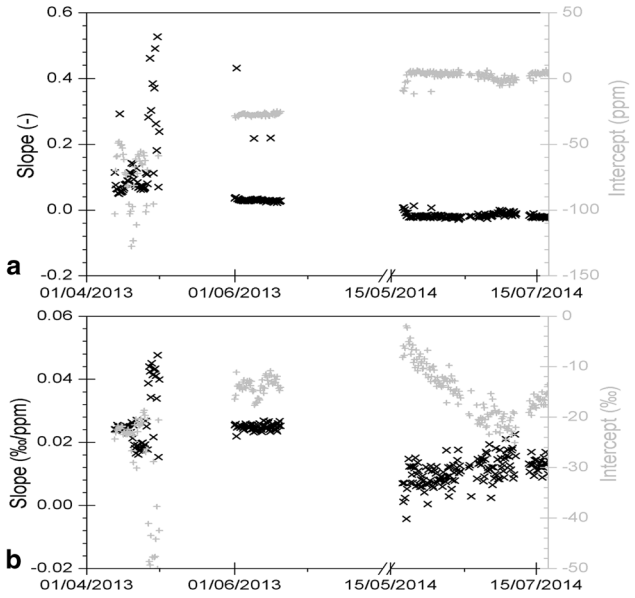

Fig. 5 Temporal stability of calibration parameters during the field monitoring period. **a** Slope $q(t)$ (*black*) and intercept $r(t)$ (*gray*) of the CO_2 concentration correction according to Eq. (1). **b** Slope $u(t)$ (*black*) and intercept $v(t)$ (*gray*) of the $\delta^{13}C$ correction according to Eq. (2)

3.3 Long-term field monitoring in an underground cavity

The raw measurements of the reference gases are presented in Fig. 4. When the analyzer was running unattended for weeks, large drifts of $\delta^{13}C$ values were observed, especially between May and July, 2014. The temporal evolution of the calibration parameters $q(t)$, $r(t)$, $u(t)$ and $v(t)$, calculated as explained above, is shown in Fig. 5. The intercepts $r(t)$ for $[CO_2]$ calibration (Fig. 5a) and $v(t)$ for $\delta^{13}C$ calibration (Fig. 5b) particularly vary with time, while the slopes $q(t)$ and $u(t)$ vary less. This is consistent with the previous observation that the concentration dependence law is randomly shifted with time, while varying monotonously on a daily timescale and keeping the same shape. Corrections that have to be applied to the raw $\delta^{13}C$ values are of large amplitude, typically on average of -8 ‰, and vary with time. This seriously decreases the accuracy and the precision of the measurements.

The raw data obtained for the tunnel and the Inner Room were processed as detailed in the previous section. The corrected CO_2 concentration and $\delta^{13}C$ values are presented in Fig. 6. CO_2 concentrations range from 400 to 1,000 ppm in the tunnel and from 530 to 800 ppm in the Inner Room. $\delta^{13}C$ values in the tunnel and in the Inner Room range from -4 to -20 ‰. In the tunnel, transient peaks of CO_2 concentration are observed on April 12, 2013, April 27, 2013, June 4, 2013, May 21, 2014 and July 11, 2014, because of the addition of CO_2 produced by the breathing of people working in the tunnel. In 2014, these

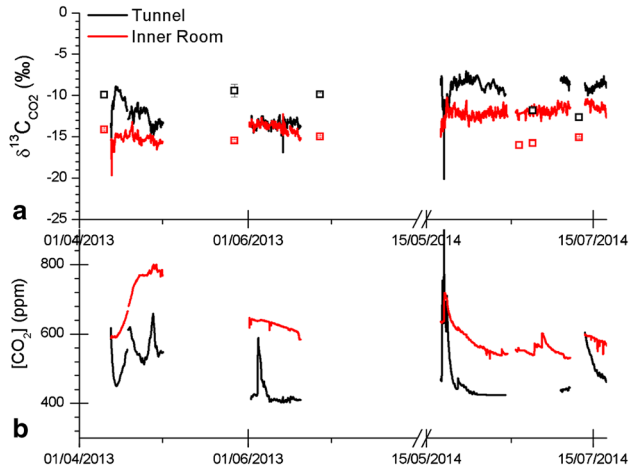

Fig. 6 Monitoring of $\delta^{13}C$ (**a**) and CO_2 concentration (**b**) in the tunnel (*black*) and the Inner Room (*red*) from April to June 2013, and May to July 2014. Reported data are corrected, 1-h averages, after 2-point calibration using reference gases measured every 8 h (cf Fig. 3). Contamination by human breathing appears as spikes in CO_2 concentrations and negative excursions in $\delta^{13}C$. *Squares* correspond to $\delta^{13}C$ values measured by CF-IRMS on discrete samples taken from the tunnel (*black*) and the Inner Room (*red*)

CO_2 peaks are also observed in the Inner Room, simultaneously with those in the tunnel. In April 2013, CO_2 concentration is observed to increase from 590 to 800 ppm in the Inner Room.

4 Discussion

4.1 Real-life performance of the IRIS analyzer and recommendations

Here we give some recommendations for in situ monitoring with the LGR CCIA-EP analyzer that can be extended to other commercial IRIS analyzers. A major focus has to be made on two points: (1) the instability of the analyzer with time and (2) the strong dependence of the measured $\delta^{13}C$ on CO_2 concentration.

4.1.1 Dealing with the temporal instability of the analyzer

It is generally noted that currently available IRIS analyzers, which display high theoretical and short-term laboratory performances, have significantly degraded performances when set in outdoor conditions. In addition to the intrinsic functioning of the analyzer and the aging of the laser, the long-term drift of the analyzer is caused by environmental parameter changes such as temperature and humidity. The sensitivity of the instrument to these varying conditions must then be carefully characterized in order to correct the raw data. In order to reduce the amplitude of corrections, we strongly advise users to work at regulating as much as possible the climatic ambiance of the analytical system. In particular, it is better to keep the water concentration as low and stable as possible, by drying sampled air and arranging the same amount of water in samples and reference gases.

Even if it is better to limit the amplitude of the corrections as much as possible, the errors induced by variable temperature or water concentration could also be considered and corrected if it is not possible to have such a well-controlled environment as in this experiment. Further experimental studies on the role of water content, and more generally on matrix effects, on $\delta^{13}C$ measurement are required for a better understanding of the induced errors.

Although not mentioned in the instruction manual and not straightforward for all users, it is recommended that the analyzer run uninterrupted in order to limit instabilities and drifts. Because of this limited stability of the instrument, the status of the analyzer and of the measurements must be checked at least every week, and the potential laser wavelength drift as well as the quality of the fit of the absorption lines must be controlled.

Even if measurements are taken every second, an integration time of several minutes up to 1 h is required during field monitoring, in order to obtain a precision better than 0.5 ‰ for $\delta^{13}C$. At the moment, the LGR CCIA-EP does not allow us to investigate faster temporal dynamics, such as high-frequency data required for eddy covariance [22]. The eddy covariance (also known as eddy correlation or eddy flux) is a key atmospheric measurement technique to measure and calculate vertical turbulent fluxes within atmospheric boundary layers.

4.1.2 Dealing with the strong concentration dependence of the isotope ratio

The large amplitude of the concentration dependence correction (up to 8 ‰ for concentrations in the range 300–800 ppm) is the major source of uncertainty. A linear approximation for the concentration dependence law is commonly used for IRIS analyzers [3, 7, 18]. The concentration dependence law obtained in this study is consistent with this approximation, as least in the limited range of concentration that was investigated. A linear law proved to perform well for calibration of $\delta^{13}C$ values during field monitoring. If fundamental spectroscopic information on the analyzer were available, this could potentially be used to determine the shape of the concentration dependence curves, based on physical principles. At present time, users have to rely on empirical laws with no spectroscopic basis.

Because of the instability of the analyzer, reference gases have to be measured frequently, at least twice a day, to track the concentration dependence law. As a linear law was used, at least two reference gases must be analyzed. These reference gases have to be carefully chosen to have the same matrix composition and to bracket the range of CO_2 concentrations of the measured air.

Even if it was not the case in this study, addition of a third reference gas, with CO_2 concentration in the measured range, would be very useful as a quality check. Regular checks of the concentration dependence law, on a weekly basis, are highly recommended in order to track any change in shape or too large drift. Validation of IRIS data against the traditional IRMS method is strongly advised. This was done here, at least with a limited number of comparison points. The agreement, and therefore the analyzer's performance, is not fully satisfactory, with a variable discrepancy of 1–4 ‰ (Fig. 6). As shown by the Allan–Werle deviation (Fig. 2a), a large uncertainty of 1–3 ‰ is expected due to the interval of 8 h between calibrations. This time interval could be reduced to 1 h, to reduce uncertainty, while keeping a reasonable consumption of reference gases and enough time for sample measurements.

4.2 Natural $\delta^{13}C$ dynamics in an underground cavity

4.2.1 Contamination by human breathing and ventilation

Large peaks in CO_2 concentration are observed in the tunnel on April 12, 2013, April 27, 2013, June 4, 2013, May 21, 2014 and July 11, 2014. They occurred when visits or field works were conducted in the tunnel and result from contamination by human respiration.

While all events increased CO_2 concentration, only the largest (on May 21, 2014) significantly modified its $\delta^{13}C$, with a small negative peak (Fig. 6). Human breath has $\delta^{13}C$ values between −20 and −23 ‰, with CO_2 concentration of several percent [23–25]. As the isotope signature of human breathing is lower than that of the background in the tunnel ($\delta^{13}C \approx -8$ to −15 ‰), the resulting $\delta^{13}C$ decreases during CO_2 peaks. In comparison, human breathing imprint in the air of the Inner Room was limited, thanks to its closed and roughly isolated door. However, the appearance of peaks in the Inner Room in May, 2014, indicates that the Inner Room became less isolated from the tunnel.

A simple mixing model between CO_2 in the tunnel air and CO_2 from human breathing can thus be used:

$$C_{\text{peak}} = x\, C_{\text{breath}} + (1 - x)\, C_{\text{tun}} \tag{5}$$

$$\delta_{\text{peak}} \cdot C_{\text{peak}} = x\, \delta_{\text{breath}} \cdot C_{\text{breath}} + (1 - x)\, \delta_{\text{tun}} \cdot C_{\text{tun}} \tag{6}$$

where x is the fraction of contamination, C_{peak} (resp. δ_{peak}) refers to peak value of CO_2 concentration (resp. carbon isotope composition), C_{tun} (resp δ_{tun}) are the corresponding values in the tunnel before the peak and C_{breath} (resp. δ_{breath}) the values for human breathing. Peak and tunnel values are taken from the measurements; carbon isotope composition of exhaled air is supposed to be −23 ‰ [23]. From Eqs. (5) and (6), CO_2 concentration in exhaled air is found to be around 15,000 ppm and the volume fraction of contamination by human breathing to be of 2 %. This value of C_{breath} is lower than the few % measured directly in the exhaled air [24], which is explained by the rapid dilution of exhaled air by the low CO_2 concentration tunnel air.

Depending on how many people are present in the tunnel, how long they stay and where they are located (or moving) with respect to the inlet of the IRIS analyzer, the shapes of the peaks may vary. A characteristic exponential decay results from the natural ventilation of the tunnel [26, 27]. These transient CO_2 perturbations by human breathing can be used to quantify the natural ventilation in the tunnel. Assuming that the source of the CO_2 perturbation is no more active after the peak and using a box model to describe the decay of the CO_2 concentration, the following equation is obtained:

$$C(t) = (C_i - C_\infty) \cdot \mathrm{e}^{-\lambda_v t} + C_\infty \tag{7}$$

where $C(t)$ is the CO_2 concentration measured in the tunnel, C_i is the maximum peak concentration, C_∞ the background CO_2 concentration in the tunnel, and λ_v is the ventilation rate (in s^{-1}). For the large CO_2 peak measured in the tunnel between May 21 and 28, 2014, $C_i = 715$ ppm is the maximum initial concentration and $C_\infty = 425$ ppm is the final stable concentration after decay (Fig. 6). The best fit of the decay curve ($R^2 = 0.91$) is obtained for a ventilation rate $\lambda_v = 1.0 \pm 0.2\ 10^{-5}\ s^{-1}$. This value of the ventilation rate is similar to the one obtained from other tracers (^{222}Rn and SF_6) for the same area of the tunnel [24]. A modified box model can then be applied to obtain the evolution of $\delta^{13}C$ in the tunnel during the decay of the CO_2 concentration:

$$\delta^{13}C(t) = \frac{(\delta_i \cdot C_i - \delta_\infty \cdot C_\infty) \cdot e^{-\lambda_v t} + \delta_\infty \cdot C_\infty}{(C_i - C_\infty) \cdot e^{-\lambda_v t} + C_\infty} \tag{8}$$

where δ_i and δ_∞ are, respectively, the peak and background carbon isotope compositions of CO_2. With the value of the ventilation rate determined above for the decay of the CO_2 concentration, an acceptable fit of the $\delta^{13}C$ evolution is obtained ($R^2 = 0.45$). This poorer fit is explained by the limited range of variation in the $\delta^{13}C$ values, not so large compared to the precision of the analyzer.

4.2.2 *Contributing fluxes of CO_2*

First, discarding the peaks of anthropogenic origin, the averaged background CO_2 concentrations in both the tunnel and the Inner Room are higher than that measured in the atmosphere (390 ± 10 ppm [28]), with 410 ± 10 and 550 ± 10 ppm, respectively. Second, the increase in CO_2 concentration observed in the Inner Room in April 2013 is lower than the more abrupt peaks of breathing contamination and occurred when there were no people working in the tunnel. These two observations have to be explained by another CO_2 source in addition to atmosphere and respiration. These CO_2 excesses indicate that a CO_2 flux is coming from the rock (hereafter referred to as geogenic CO_2) and allow us to estimate this flux. A simple mass balance leads to the differential equation governing the CO_2 concentration in the tunnel or the Inner Room:

$$\frac{\mathrm{d}C}{\mathrm{d}t} = \frac{S}{V}\frac{RT}{P_a M_{CO_2}}\Phi - \lambda_v (C - C_a) \tag{9}$$

where C is the CO_2 concentration in the tunnel or in the Inner Room, S (resp. V) is the surface area of the walls (in m^2) (resp. the volume in m^3), R is the ideal gas constant, T is the tunnel temperature (in K), P_a is the average atmospheric pressure (850 hPa at the Roselend Natural Laboratory), $M_{CO_2} = 44$ g mol^{-1} is the molecular mass of CO_2, $C_a = 380$ ppm is the CO_2 concentration in the atmosphere, λ_v is the ventilation rate (in s^{-1}), and Φ is the flux of CO_2 released by the rock (in g m^{-2} day^{-1}). At steady state, the flux Φ can be calculated from the average CO_2 concentration C_∞ that is measured in the tunnel or in the Inner Room according to the following equation:

$$\Phi = \frac{V}{S}\frac{P_a M_{CO_2}}{RT}\lambda_v\,(C_\infty - C_a) \tag{10}$$

Using a ventilation rate of $1.0 \times 10^{-5}\ s^{-1}$ in the tunnel, as determined previously, a lower value of $3 \times 10^{-6}\ s^{-1}$

in the Inner Room (according to [26]), and steady state concentrations of 410 and 550 ppm in the tunnel and the Inner Room, respectively, we obtained CO_2 fluxes of 0.02 g m^{-2} day^{-1} in the tunnel and 0.05 g m^{-2} day^{-1} in the Inner Room. These values are 5–10 times lower than the one of 0.11 g m^{-2} day^{-1} previously obtained in a borehole (Perm 4) that laterally extends 2.3 m into the host rock from the tunnel wall [6]. This difference is explained by the difference of the spatial scale of the surfaces contributing to the CO_2 flux (0.06 m^2 for the borehole, 61 m^2 for the Inner Room, and 98 m^2 for the portion of tunnel where the analyzer is installed and which is delimited by plastic curtains [26]). While the small borehole Perm 4 represents a high CO_2 flux end-member, rock areas with high and low fluxes (corresponding chiefly to matrix-dominated and fracture-dominated areas) are averaged in the larger tunnel and Inner Room.

4.2.3 *Sources of CO_2*

Carbon isotope composition gives insights into the sources of CO_2 production and release from rocks. The data obtained in this study using the IRIS analyzer, in both the tunnel and the Inner Room, are plotted in a Keeling plot ($\delta^{13}C$ vs. $1/[CO_2]$, Fig. 7). Discrete air samples were also taken for CF-IRMS analysis from borehole Perm 4 and from Chamber C. Chamber C is a 60 m^3 cavity, similar to the Inner Room, but isolated from the tunnel by an airtight wall. Both Chamber C and borehole Perm 4 were completely isolated from the tunnel during the experiment, which allows CO_2 to accumulate and leads to concentrations higher than those obtained in the tunnel and in the Inner Room. Both Chamber C and borehole Perm 4 remained free of contamination by human breathing.

CO_2 in these four environments, tunnel, Inner Room, Chamber C and borehole Perm 4 consists in a mixing between atmospheric CO_2 and geogenic CO_2. This two end-member mixing corresponds to a linear trend in a Keeling plot. This is indeed what is observed here with the whole data set (Fig. 7). The carbon isotope composition of the CO_2 released by the rock is given by the intercept of the mixing line with the vertical axis, following [29, 30]. The obtained value of $\delta^{13}C = -25 \pm 3$ ‰ is consistent with that of -23.7 ± 0.5 ‰ obtained from a flux measurement performed in borehole Perm 4 [6].

Such isotope composition is at first order consistent with that of the CO_2 degassed from HCO_3^- dissolved in water dripping from the roof of the tunnel (with pH in the range 7.7–8.1) [6]. The $\delta^{13}C$ value of dissolved HCO_3^- was measured at -10.9 ± 1.5 ‰ [14], and the isotope fractionation at 7 °C between CO_2 and dissolved HCO_3^- is −9.6 ‰ [31, 32], which leads to a $\delta^{13}C$ value of -20.5 ± 1.5 ‰ for degassed CO_2. This range in isotope composition of

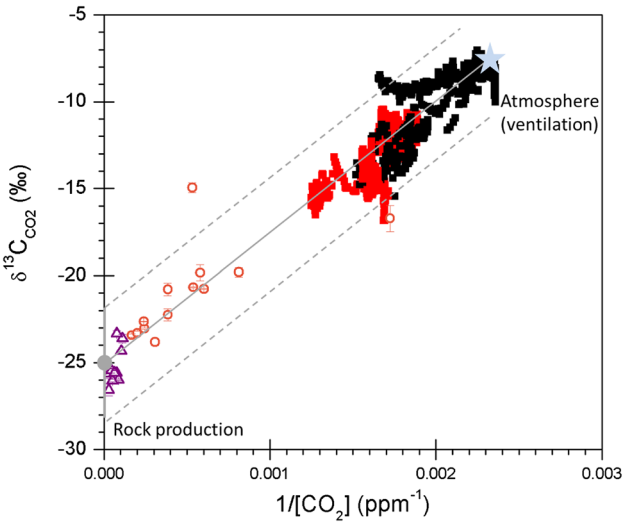

Fig. 7 Keeling plot (CO_2 carbon isotope composition versus the inverse of the CO_2 concentration) from long-term in situ monitoring in the tunnel (*black squares*) and the Inner Room (*red squares*) with the LGR CCIA-EP analyzer (IRIS). Reported data are corrected 1-h averages from Fig. 6, except for periods when the tunnel was contaminated by human breathing and that have been removed. Measurements of $\delta^{13}C$ by CF-IRMS in samples taken from chamber C (*red circles*) and borehole Perm 4 (*purple triangles*) are also reported. The linear trend in the data highlighted by the *gray lines* corresponds to a 2 end-member mixing between atmospheric air (*blue star*, 430 ± 20 ppm CO_2, $\delta^{13}C = -7.7 \pm 0.5$ ‰, values determined from the Keeling plot and in the upper range from that given in [28]) and pore space air (≥10,000 ppm CO_2, $\delta^{13}C = -25 \pm 2$ ‰), this later value being determined from the intercept of the linear regression (*gray circle*)

HCO_3^- is consistent with production by microbial and plant respiration of C3 organic matter [33], in the soil at the surface and in the 55 m of rocks above the tunnel, with some contribution from weathering of carbonate minerals [34].

No clear seasonal variability can be seen in the obtained data, neither for CO_2 concentration nor for $\delta^{13}C$ values (Fig. 6). In the Inner Room, no change in $\delta^{13}C$ occurred during the increase in CO_2 concentration observed April 2013. This suggests an increase in the intensity of the CO_2 flux released by the rock without the addition of another CO_2 source.

Further monitoring would be required to investigate in more detail the temporal variability of carbon isotope composition in dissolved HCO_3^-, degassed CO_2, carbon sources and transport processes.

5 Conclusion

The performance assessment of the commercial IRIS analyzer LGR CCIA-EP shows that despite fast measurement

rate (1 Hz) and response time, an integration time of several minutes up to 1 h is required to obtain a precision better than 0.5 ‰ on $\delta^{13}C$, almost comparable to IRMS performance and required for discrimination of natural carbon sources. We emphasize the difficulties encountered by any user to process, correct and calibrate raw data. The two main sources of uncertainty that have to be carefully taken into account are the dependence of $\delta^{13}C$ on CO_2 concentration and the temporal instability of the analyzer.

As shown here as well as in other works using commercial IRIS analyzers [3, 7], there is a need for development and validation of data processing schemes, available to the users' community, in order to ensure accurate and reliable measurements.

IRIS analyzers offer an unprecedented possibility of long-term in situ monitoring of CO_2 isotope composition in a variety of natural environments. This is very promising for understanding the spatial and temporal dynamics of $\delta^{13}C$ and carbon sources, for example, by investigating the time variability of Keeling plot intercept, as it is done for ecosystem respiration [30].

The presented instrument and application study are relevant for monitoring underground cavities, whether to understand CO_2 dynamics in visited and/or painted caves for preservation purposes [35] or to understand paleoclimate recording in speleothems [36]. However, in these applications with high CO_2 concentrations or CO_2 concentrations varying in a large range, using IRIS, remains very challenging at the moment. Further work would be required to validate protocols and data processing schemes adapted to these conditions and to the various commercial IRIS analyzers.

We presented in situ monitoring of CO_2 and $\delta^{13}C$ at the Roselend Natural Laboratory with a high temporal resolution and for a total of 3 months between April 2013 and July 2014. Transient peaks of CO_2 concentration are due to contamination by human breathing and allow us to quantify the ventilation rate. Discarding these peaks, the CO_2 background higher than the atmospheric one allows us to quantify a net CO_2 flux that is shown to be contributed by the rock. $\delta^{13}C$ of this geogenic CO_2 flux is determined with a Keeling plot and is consistent with production by plant and microbial respiration at the surface as well as production from weathering of carbonate minerals in the rock. A one-month transient increase in CO_2 concentration is observed, due to an increase in the geogenic CO_2 flux, but no diurnal or seasonal variability of CO_2 and $\delta^{13}C$ is detected from the measurements.

Acknowledgments We thank Carine Chaduteau for her help with IRMS measurements. We thank Doug Baer, Feng Dong and other people at Los Gatos Research for their availability, advice and help in using this analyzer in specific conditions. Thanks go to Didier Mondelain for introducing us to laser-based isotope analysis and to Allan–Werle variance. Benjamin Richard is being thanked for the systematic analysis of the analyzer performance in the laboratory. We thank Erik Kerstel and an anonymous reviewer for their thoughtful comments that helped improving the manuscript. This is IPGP Contribution Number 3574.

References

1. D.R. Bowling, S.D. Sargent, B.D. Tanner, J.R. Ehleringer, Agric. For. Meteorol. **118**, 1 (2003)
2. A.L. Rizzo, H.-J. Jost, A. Caracausi, A. Paonita, M. Liotta, M. Martelli, Geophys. Res. Lett. **41**, 2014GL059722 (2014)
3. X.F. Wen, Y. Meng, X.Y. Zhang, X.M. Sun, X. Lee, Atmos. Meas. Tech. **6**, 1491 (2013)
4. D.W.T. Griffith, N.M. Deutscher, C. Caldow, G. Kettlewell, M. Riggenbach, S. Hammer, Atmos. Meas. Tech. **5**, 2481 (2012)
5. G. Friedrichs, J. Bock, F. Temps, P. Fietzek, A. Kortzinger, D.W.R. Wallace, Limnol. Oceanogr. Methods **8**, 539 (2010)
6. S. Guillon, E. Pili, P. Agrinier, Appl. Phys. B Lasers Opt. **107**, 449 (2012)
7. P. Sturm, B. Tuzson, S. Henne, L. Emmenegger, Atmos. Meas. Tech. **6**, 1659 (2013)
8. B. Tuzson, J. Mohn, M.J. Zeeman, R.A. Werner, W. Eugster, M.S. Zahniser, D.D. Nelson, J.B. McManus, L. Emmenegger, Appl. Phys. B Lasers Opt. **92**, 451 (2008)
9. S. Guillon, T.M. Vu, E. Pili, P.M. Adler, Water Resour. Res. **49**, 2801 (2013)
10. A. Kammer, B. Tuzson, L. Emmenegger, A. Knohl, J. Mohn, F. Hagedorn, Agric. For. Meteorol. **151**, 39 (2011)
11. S. Laukenmann, D. Polag, H. Heuwinkel, M. Greule, A. Gronauer, J. Lelieveld, F. Keppler, Eng. Life Sci. **10**, 509 (2010)
12. J.U.L. Baldini, L.M. Baldini, F. McDermott, N. Clipson, J. Cave Karst Stud. **68**, 4 (2006)
13. C. Batiot-Guilhe, J.L. Seidel, H. Jourde, O. Hebrard, V. Bailly-Comte, Int. J. Speleol. **36**, 51 (2007)
14. E. Pili, M. Dellinger, L. Charlet, P. Agrinier, F. Chabaux, P. Richon, Geochim. Cosmochim. Acta **73**, A1029 (2009)
15. D.S. Baer, J.B. Paul, M. Gupta, A. O'Keefe, Proc. SPIE Int. Soc. Opt. Eng. **4817**, 167 (2002)
16. P. Werle, Appl. Phys. B Lasers Opt. **102**, 313 (2011)
17. P. Werle, R. Mucke, F. Slemr, Appl. Phys. B **57**, 131 (1993)
18. P. Sturm, A. Knohl, Atmos. Meas. Tech. **3**, 67 (2010)
19. X.F. Wen, X.H. Lee, X.M. Sun, J.L. Wang, Y.K. Tang, S.G. Li, G.R. Yu, J. Atmos. Ocean. Technol. **29**, 235 (2012)
20. A.-S. Provost, P. Richon, E. Pili, F. Perrier, S. Bureau, EOS, transactions. Am. Geophys. Union **85**, 113 (2004)
21. C. Stowasser, A.D. Farinas, J. Ware, D.W. Wistisen, C. Rella, E. Wahl, E. Crosson, T. Blunier, Appl. Phys. B **116**, 255 (2014)
22. T.J. Griffis, S.D. Sargent, X. Lee, J.M. Baker, J. Greene, M. Erickson, X. Zhang, K. Billmark, N. Schultz, W. Xiao, N. Hu, Bound. Layer Meteorol. **137**, 307 (2010)
23. S. Epstein, L. Zeiri, Proc. Natl. Acad. Sci. USA **85**, 1727 (1988)
24. S.N. Andreev, E.S. Mironchuk, I.V. Nikolaev, V.N. Ochkin, M.V. Spiridonov, S.N. Tskhai, Appl. Phys. B Lasers Opt. **104**, 73 (2011)
25. E.R. Crosson, K.N. Ricci, B.A. Richman, F.C. Chilese, T.G. Owano, R.A. Provencal, M.W. Todd, J. Glasser, A.A. Kachanov, B.A. Paldus, T.G. Spence, R.N. Zare, Anal. Chem. **74**, 2003 (2002)

26. F. Perrier, P. Richon, J.C. Sabroux, Sci. Total Environ. **350**, 136 (2005)
27. P. Richon, F. Perrier, J.C. Sabroux, M. Trique, C. Ferry, V. Voisin, E. Pili, J. Environ. Radioact. **78**, 179 (2005)
28. I.T. van der Laan-Luijkx, S. van der Laan, C. Uglietti, M.F. Schibig, R.E.M. Neubert, H.A.J. Meijer, W.A. Brand, A. Jordan, J.M. Richter, M. Rothe, M.C. Leuenberger, Atmos. Meas. Tech. **6**, 1805 (2013)
29. C.D. Keeling, Geochim. Cosmochim. Acta **24**, 277 (1961)
30. D.E. Pataki, J.R. Ehleringer, L.B. Flanagan, D. Yakir, D.R. Bowling, C.J. Still, N. Buchmann, J.O. Kaplan, J.A. Berry, Glob. Biogeochem. Cycles **17**, 1–14 (2003)
31. P. Deines, D. Langmuir, R.S. Harmon, Geochim. Cosmochim. Acta **38**, 1147 (1974)
32. W.G. Mook, J. Bommerso, W. Staverma, Earth. Planet. Sci. Lett. **22**, 169 (1974)
33. C.T. Lai, A.J. Schauer, C. Owensby, J.M. Ham, J.R. Ehleringer, J. Geophys. Res. Atmos. **108**, 1–14 (2003)
34. E. Pili, S. Guillon, P. Agrinier, M. Dellinger: Mineral. Mag. **75**(3), 1644 (2011)
35. F. Bourges, P. Genthon, D. Genty, M. Lorblanchet, E. Mauduit, D. D'Hulst, Sci. Total Environ. **493**, 79 (2014)
36. D.M. Tremaine, P.N. Froelich, Y. Wang, Geochim. Cosmochim. Acta **75**, 4929 (2011)